Applied Physics Letters PERSPECTIVE pubs.aip.org/aip/apl

Recent progress in indoor photovoltaics based on all-inorganic perovskites

Cite as: Appl. Phys. Lett. **127**, 040502 (2025); doi: 10.1063/5.0275628
Submitted: 14 April 2025 · Accepted: 14 July 2025 ·
Published Online: 30 July 2025

View Online Export Citation CrossMark

Yu Qi, Wenjie Xu, Yanhui Lou,[a] and Lai Feng[a]

AFFILIATIONS

Soochow Institute for Energy and Materials Innovation (SIEMIS), School of Energy, Soochow University, Suzhou 215006, China and Jiangsu Key Laboratory of Advanced Carbon Materials and Wearable Energy Technologies, Jiangsu Key Laboratory of Advanced Negative Carbon Technologies Soochow University, Suzhou 215006, China

Note: This paper is part of the Special Topic, High-Performance Thin-Film Indoor Photovoltaics.
[a]**Authors to whom correspondence should be addressed:** yhlou@suda.edu.cn and fenglai@suda.edu.cn

ABSTRACT

The rapid proliferation of Internet of Things (IoT) devices, ranging from smart sensors to wearable electronics, has intensified the demand for sustainable energy solutions capable of powering low-power electronics under indoor illumination. In this context, indoor photovoltaics (IPVs) emerge as a promising technology to enable continuous electricity supply for autonomous IoT systems. To maximize energy harvesting efficiency under indoor conditions, IPV absorbers require an optimal bandgap of 1.7–1.9 eV to match the spectral characteristics of indoor environments as well as high defect tolerance to minimize the defect-induced recombination. These requirements position all-inorganic perovskites (AIPs), particularly $CsPbI_3$ and $CsPbI_2Br$, as superior candidates for IPVs compared to conventional silicon absorbers. This review summarizes recent advancements on AIP-based IPVs, which lead to indoor efficiency exceeding 40%, far surpassing conventional silicon cells. This review also examines a series of synergistic efforts toward the AIP-based IPVs with high performance, further discusses the existing challenges and provides multiple perspectives regarding the future optimization of AIP-based IPVs for practical applications.

I. INTRODUCTION

The widespread adoption of Internet of Things (IoTs) technology has bridged the physical and digital worlds through interconnected sensors and networks, revolutionizing daily life and industrial productivity. This rapid proliferation of IoT systems, particularly those integrating flexible, wearable, and wireless sensors on a massive scale, necessitates sustainable and cost-effective power solutions.[1–4] Conventional rechargeable batteries and wired power systems suffer from intrinsic limitations in scalability, maintenance, and environmental sustainability. While batteries offer portability, their finite lifespan and frequent replacement requirements pose critical challenges for large-scale IoT deployments. In contrast, photovoltaic devices, as self-sustaining energy harvesters, present a carbon-neutral alternative capable of continuously powering IoT devices under ambient indoor illumination.[5–8]

Indoor lighting environments, predominantly illuminated by fluorescent lamps (FLs) and white light-emitting diodes (WLEDs), exhibit distinct spectral characteristics compared to natural sunlight. These artificial light sources emit narrow-band visible spectra (380–780 nm) with intensities approximately three orders of magnitude lower (~300 μW cm^{-2}) than standard solar irradiance (100 mW cm^{-2}).[9,10] Consequently, optimal materials for indoor photovoltaics (IPVs) require wide bandgaps (E_g = 1.7–2.0 eV) to maximize photon absorption within this spectral range as well as high defect tolerance to minimize defect-induced charge recombination. However, traditional photovoltaic materials, such as crystalline silicon (1.1 eV),[11] CuInGaSe (1.0–1.7 eV),[12] and Cu_2ZnSnS_4 (1.5 eV),[13] exhibit suboptimal bandgap alignment with indoor spectra and low defect tolerance, creating opportunities for alternative semiconductors.

Recent studies revealed that single-junction IPVs can reach a S-Q efficiency of ~57% with a V_{OC} up to 1.51 V at an E_g of 1.82–1.96 eV under indoor lighting (300 lux).[14] Thus, AIPs with wide E_g that well match the indoor light spectra are optimal for IPVs.[15] In addition, AIPs exhibit high defect tolerance, manifesting as minimized defect density through various passivation strategies.[16–18] To date, the best IPVs based on $CsPbI_3$ (1.73 eV) achieved a high efficiency of 41.21% (V_{OC} = 1.07 V) under 1062 lux WLED illumination, surpassing other wide-bandgap devices such as amorphous silicon (a-Si:H, 36% at 3000 lux)[19,20] and organic photovoltaics (OPV, 35% at 1000 lux).[21] Thus, AIPs have been considered as viable alternatives for IoT devices requiring sustainable operation in dim environments.

This review systematically evaluates recent efforts toward high-performance IPVs based on AIPs, including crystallization regulation and defect suppression through additive engineering, anti-solvent strategies, interfacial modification, HTL evolution, and absorber tuning (see Fig. 1). Furthermore, this review delineates remaining challenges and outlines future directions for achieving high-performance AIP-based IPVs tailored to IoT applications.

II. ADDITIVE ENGINEERING

Extensive studies have demonstrated that additive engineering serves as an effective strategy to modulate the crystallinity of AIP films. Current approaches primarily involve incorporating functional additives into precursor solutions to regulate primary crystallization kinetics (see Table I).[21] In recent years, organic ionic additives have been widely employed to modify the thermal crystallization kinetics of AIPs. Pioneering work by Jung's group (2020–2022) systematically introduced methylammonium iodide (MAI) and tetramethylammonium chloride (TMACl) into $CsPbI_2Br$ precursor solutions.[22,23] It was observed that these additives obviously retarded the crystallization of AIP and resulted in improved film quality of AIP with minimized pin-holes and reduced defects. The authors proposed that the organic cation and Cs^+ competitively go into the lattice of perovskite upon thermal annealing, and the hybrid perovskite (i.e., $MAPbI_2Br$) temporarily present serves as a template for remaining Cs^+ substitution to completely form $CsPbI_2Br$ [see Fig. 2(a)]. The resultant photovoltaic devices with normal architectures achieved remarkable PCEs of 23.51% and 27.16%, respectively, under WLED illumination (1000 lux). Bahadur *et al.* utilized multifunctional 2-amino-5-nitrothiazole (ANT) to regulate crystallization and passivate defects of $CsPbI_2Br$ film. ANT additive forms an intermediate phase ($CsI:DMSO:PbI_2$:ANT) and slows crystal growth time, leading to high quality of film with larger crystals and dense morphology. The optimized device demonstrated a PCE of 29.47% under indoor WLED illumination (1000 lux).[24] In another work, Im *et al.* demonstrated that dimethylammonium iodide (DMAI) enhances the solubility of $CsPbI_2Br$ precursors, thereby retarding crystallization to promote large-grain formation.[25] The normal devices with ITO/SnO_2/$CsPbI_2Br$(DMAI)/P3HT/Au configuration achieved PCEs of 35.22% (0.096 cm^2), 35.08% (1 cm^2), and 29.80% (25 cm^2) under 1000 lux illumination while maintaining 1000-h stability in the ambient environments. Further advancements by Du *et al.* introduced ionic liquid additives, specifically 1-ethyl-3-methylimidazolium hydrogen sulfate ($EMIMHSO_4$), which facilitated *in situ* formation of PbI_2-$EMIMHSO_4$ intermediates during ambient printing of $CsPbI_3$ precursor film.[26] This dual-functional additive not only improved crystallization but also passivated AIP defects through strong coordination with the under-coordinated Pb^{2+} and iodine vacancies (V_I), enabling a champion efficiency of 37.24% under indoor lighting (1000 lux). Li *et al.* added methyl acetate amine (MAAc) into the precursor solution of $CsPbI_2Br$, and an intermediate phase $MA_xCs_{1-x}PbI_2Br$ was formed through hydrogen bonding to assist crystallization, slowing down the crystallization rate and enabling large-area and low defect AIP thin films. The device exhibited high efficiency of 38.24% under 1000 lux illumination.[27] On the other hand, cytidine 5′-monophosphate (5′-CMP), a natural nonionic organic compound with multiple passivation sites, was reported as an effective additive for $CsPbI_2Br$ crystallization.[28] As illustrated in Fig. 2(b), 5′-CMP may regulate the formation of colloidal precursors, and hence facilitate the crystallization of $CsPbI_2Br$, resulting in high-quality AIP film with larger grains, higher crystallinity, reduced tensile stress, mitigated defects, improved electronic property and reduced modulus. The inverted devices delivered a PCE of 33.22% under comparable indoor conditions [Fig. 2(c)], considerably surpassing that of the control devices (26.66%).

Despite these advances, there remains uncertainty regarding the effect of organics on device stability. Thus, inorganic salts emerged as alternative additives for crystallization control. Jin *et al.* demonstrated that CsCl incorporation led to improved $CsPbI_2Br$ crystallization with larger grains and reduced defect density, achieving a champion PCE of 25.53% with a high V_{OC} of 1.08 V under indoor lighting (1000 lux) [Figs. 2(d) and 2(f)].[29] Parallel investigations by Tan *et al.* revealed that lead acetate ($Pb(Ac)_2$) additive can optimize the growth orientation of crystallites and reduce defect density in $CsPbI_2Br$ films. When integrated with PM6-based hole-transport layer (HTL), the resulting

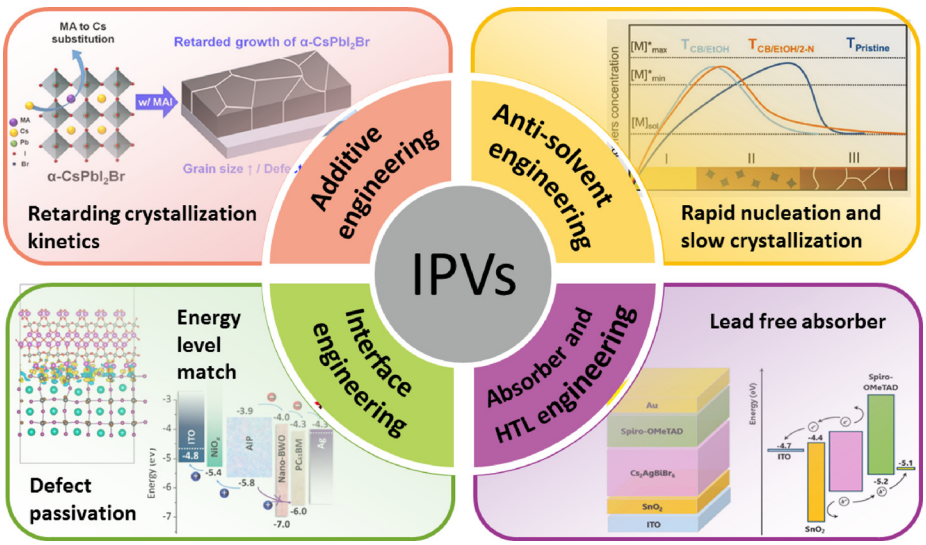

FIG. 1. Summary of recent advances for AIP-based IPVs.

TABLE I. Recently reported IPV-performances based on additive strategies.

Date	Device structure	V_{oc} (V)	J_{sc} (μA cm^{-2})	*FF* (%)	PCE (%)	Light source/intensity	Strategy	Ref.
2020	ITO/SnO_2/$CsPbI_2Br$/Spiro-OMeTAD/Au	0.95	114	70	23.51	WLED/6500 K 1000 lux	MAI additive	22
2021	ITO/SnO_2/$CsPbI_2Br$/TFB/P3HT/Au	0.94	122.0	77	27.16	WLED/6500 K 1000 lux	TMACl additive	23
2021	ITO/SnO_2/$CsPbI_2Br$/Spiro-OMeTAD/Au	1.08	117.5	65	25.53	WLED/6500 K 1000 lux	CsCl additive	29
2022	FTO/TiO_2/$CsPbI_3$/Spiro-OMeTAD/Au	0.988	177	77.8	37.24	Cool WLED 1000 lux	$EMIMHSO_4$ additive	26
2022	ITO/SnO_2/$CsPbI_2Br$/P3HT/Au	1.08/1.11/1.13	26.09/65.13/130.22	80.75/80.27/79.96	34.15/34.74/35.22	WLED/6500 K 200/500/1000 lux	DMAI additive	25
2022	ITO/SnO_2/$CsPbI_2Br$/PM6/MoO_3/Ag	1.15	118	81.86	33.68	WLED/3000 K 1000 lux	$Pb(Ac)_2$ additive	30
2024	(ITO/SnO2/ZnO/CsPbI2Br/P3HT/Au	0.965	158	73.54	29.47	WLED/3200 K	ANT additive	24
2024	ITO/SnO_2/$CsPbI_2Br$//P3HT/Au	~1.22	~130		38.24	1000 lux	MAAc aditive	27
2024	ITO/Spiro-OMeTAD@PTAA/$CsPbI_2Br$/$PC_{61}BM$/BCP/Ag	1.02	151	81.3	33.22	WLED/6500 K 1000 lux	5′-CMP additive	28

devices with normal structure attained a PCE of 33.68% with a remarkable V_{OC} of 1.15 V and high *FF* of 81.86% under dim illumination (1000 lux).[30]

III. ANTI-SOLVENT ENGINEERING

Anti-solvents can facilitate rapid solvent extraction from precursor film to induce supersaturation, thereby controlling nucleation and crystal growth processes.[31–33] The approach as a critical strategy is utilized to regulate the crystallization kinetics of organic–inorganic hybrid perovskite films. Building on this demonstrated capability in hybrid systems, the strategy is applied to AIP films to improve crystallinity and overall quality of the films. A foundational study by Ghosh *et al.* employed diethyl ether and chlorobenzene (CB) as anti-solvents for $CsPbIBr_2$ film fabrication.[34] It was found that the diethyl ether treatment could better facilitate the formation of a compact and low-defect film with suppressed Pb^0 defects and reduced crystallographic disorder [see Fig. 3(a)]. The optimal devices with normal architecture achieved a PCE of 14.1% under 1000 lux indoor illumination. Nevertheless, this work highlighted a critical limitation: conventional anti-solvent strategies exhibit limited capability in defect passivation during crystallization. Further progress has been achieved through a combined anti-solvent and molecular additive engineering. In 2021, as described in Figs. 3(b) and 3(c), Wang *et al.* innovatively introduced ethanol (EtOH) solution of ammonium oxalate hydrate [$(NH_4)_2C_2O_4{\cdot}H_2O$: 2 mg mL^{-1}] to promote secondary crystallization of $CsPbI_2Br$ film.[35] As a result, the normal devices achieved a PCE of 28.48% under indoor lighting conditions (FL/1000 lux). A parallel study revealed that the post-treatment on the surface of $CsPbI_2Br$ film by using IPA solution of fluorinated ionic liquid 3-(trifluoromethyl) benzylamine (CFBA: 3 mg/mL) also induced the secondary crystallization of AIP.[36] Detailed analysis showed that this strategy could simultaneously enhance the crystallinity, grain size, surface coverage, and moisture resistance of AIP films due to strong interactions between the trifluoro (-CF_3)/amine groups of CFBA and AIP defects (i.e., under-coordinated Pb^{2+} and halide vacancies), thus boosting the indoor efficiency from 18.35% to 23.24% under WLED lighting (1000 lux). Another representative study incorporated phthalimide (2-N) into the anti-solvent of EtOH/CB.[37] It was proposed that the planar conjugated structure of 2-N is conductive for the strong π-π interactions with remaining solvent molecules (e.g., DMF/DMSO), enabling precise control over solvent evaporation dynamics. As depicted in Figs. 3(d) and 3(e), this strategy thus realized the synchronous regulation of rapid initial nucleation followed by slow, ordered crystal growth of AIP. The resultant $CsPbI_3$ films exhibited millimeter-scale grains with low intra-grain defects. When integrated into photovoltaic devices, a record indoor PCE of 40.07% could be achieved under WLED illumination (2956 K/1062 lux), setting a new benchmark for AIP-based IPVs. All recently reported IPV-performances based on anti-solvent strategies are listed in Table II.

IV. INTERFACE ENGINEERING

Extensive investigations revealed that interfacial defects at grain boundaries and surfaces dominate non-radiative recombination in AIP films. Interface engineering strategies, particularly through functional material design at critical heterojunctions (AIP/HTL or AIP/ETL), have emerged as effective approaches to mitigate interfacial defects.[38–40] Typically, the macromolecular characteristics of polymers—including tunable functional groups, solution processability, and mechanical robustness—endow them with unique advantages for

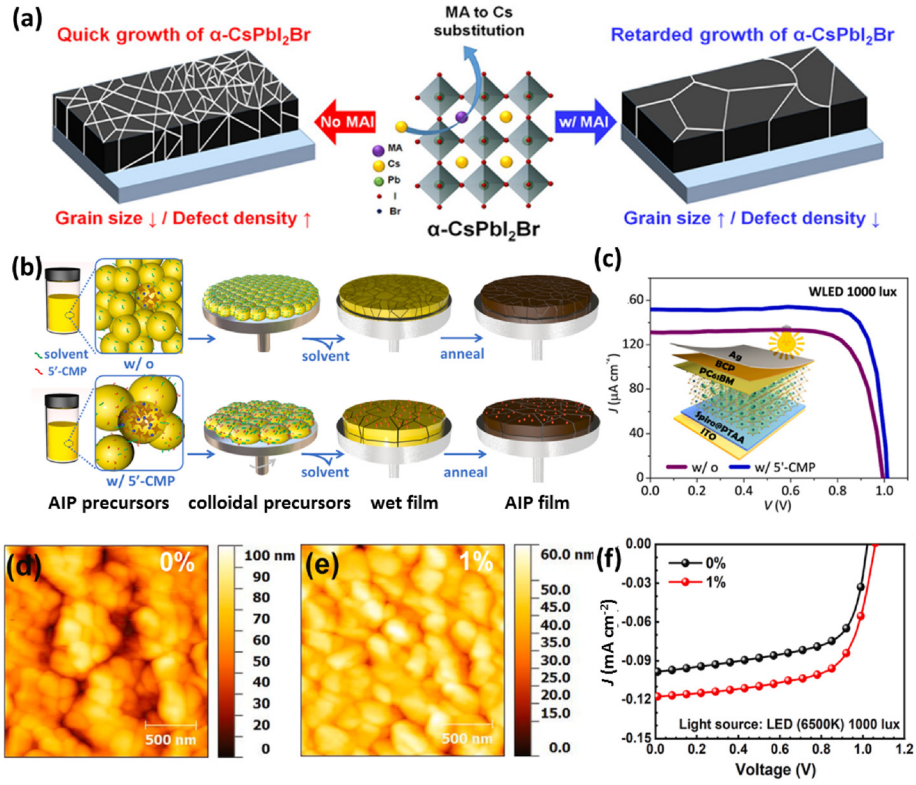

FIG. 2. (a) Schematic illustration of $CsPbI_2Br$ film formation with MAI.[22] Reproduced with permission from Kim *et al.*, ACS Appl. Mater. Interfaces **12**(32), 36228–36236 (2020). Copyright 2020 American Chemical Society. (b) Schematic depiction of $CsPbI_2Br$ film formation from colloidal precursors with 5′-CMP, and (c) indoor *J–V* characteristics of inverted devices.[28] Reproduced with permission from Xu *et al.*, Chem. Eng. J. **480**, 147946 (2024). Copyright 2024 Elsevier. (d) and (e) AFM images of $CsPbI_2Br$ films without and with 1% CsCl, and (f) indoor *J–V* characteristics of normal devices.[29] Reproduced with permission from Jin *et al.*, J. Power Sources **512**, 230481 (2021). Copyright 2021 Elsevier.

interfacial passivation. Chung *et al.* pioneered this approach by employing carboxylated polythiophene (P3CT) at the $CsPbI_2Br$/HTL interface.[41] The carboxyl groups coordinated with under-coordinated Pb^{2+} ions, suppressing interfacial recombination centers, while the π-conjugated backbone facilitated hole transport. This strategy enabled normal-structured devices to achieve a PCE of 27.47% under dim light. Subsequent advancements by Liu *et al.* demonstrated that hyperbranched poly(amidoamine) (PAMAM) dendrimers, featuring multidentate amine terminals, could comprehensively passivate interfacial defects through spatial charge compensation.[42] The optimized devices based on $CsPbI_2Br$ attained a PCE of 35.71% with a high V_{OC} of 1.06 V and remarkable *FF* of 84.39% under indoor lighting, highlighting the critical role of molecular architecture of polymer passivator in defect mitigation.

It was also found that ionic organics could enable simultaneous defect passivation and crystallization control in AIP films. In 2023, Wang *et al.* developed an amino naphthalene sulfonate (4A1N)-based strategy for modification of buried interface $TiO_2/CsPbI_3$,[43] where the synergistic effects of sulfonic acid groups (defect passivation sites) and amino moieties (crystallization regulation) led to reduced interfacial recombination loss and large shunt resistance [Figs. 4(a) and 4(b)]. This effort led to an optimal PCE of 32.54% under dim lighting (522 lux). Another breakthrough including trifluoroacetamidine (TFA) passivators reported effective suppression of iodide vacancies (V_I) while forming moisture-resistant surface layers, delivering a PCE of 39.78% under cool WLED lighting (1200 lux).[44] Systematic studies on thiophene-based salts further demonstrated that 2,5-thiophenedicarboxylic acid (TDCA) could effectively passivate the interfacial defects [i.e., under-coordinated Pb^{2+} and iodide vacancy (V_I)] at the $CsPbI_{2.25}Br_{0.75}$/HTL interface, leading to evaluated valence band position on the AIP surface and hence a better interfacial energy band alignment [see Figs. 4(c) and 4(d)]. As illustrated in Fig. 4(e), the optimal devices achieved PCEs of 29.56%–32.41% with remarkable V_{OC} up to 1.23 V under dim lighting (200–1000 lux).[45]

Another concern focused on the mismatched energy levels at the AIP/HTL or AIP/ETL interfaces. As the offset between the conduction-band minimum (CBM) of $CsPbI_3$ or $CsPbI_2Br$ (−3.8 to −3.9 eV) and LUMO (-4.3 eV) of $PC_{61}BM$ is as large as 0.5–0.4 eV, it indicates significant energy loss during the electron transfer process.[48] To address this concern, tailored interfacial modifications are necessary. As described in Figs. 4(f) and 4(g), Wang *et al.* innovatively employed propylamine hydrochloride (PACl) post-treatment to induce n-type doping on the $CsPbI_3$ surface, thereby aligning energy levels and reducing interfacial voltage loss.[46] This approach yielded inverted devices with decent PCEs up to 38.93% under WLED lighting (1000 lux). Additional representative work by our group introduced inorganic Bi_2WO_4 nanosheets (Nano-BWO) at the $CsPbI_2Br/PC_{61}BM$ interface, establishing gradient heterojunctions through staggered band alignment and hence significantly enhanced electron extraction efficiency [see Fig. 4(h)].[47] Meanwhile, a combined experimental and DFT analysis revealed the remarkable defect passivation effect of Nano-BWO due to the evident interaction at the interface dominated by Pb-O and Bi-I/Bi-Br bonds [see Fig. 4(i)]. This strategy thus enabled inverted devices with champion PCEs of 30.43% (rigid) and 24.50% (flexible) under 1000 lux conditions [Fig. 4(j)]. Xu *et al.* utilized benzyl chloromethyl sulfide (BCMS) molecules to *in situ* induce surface

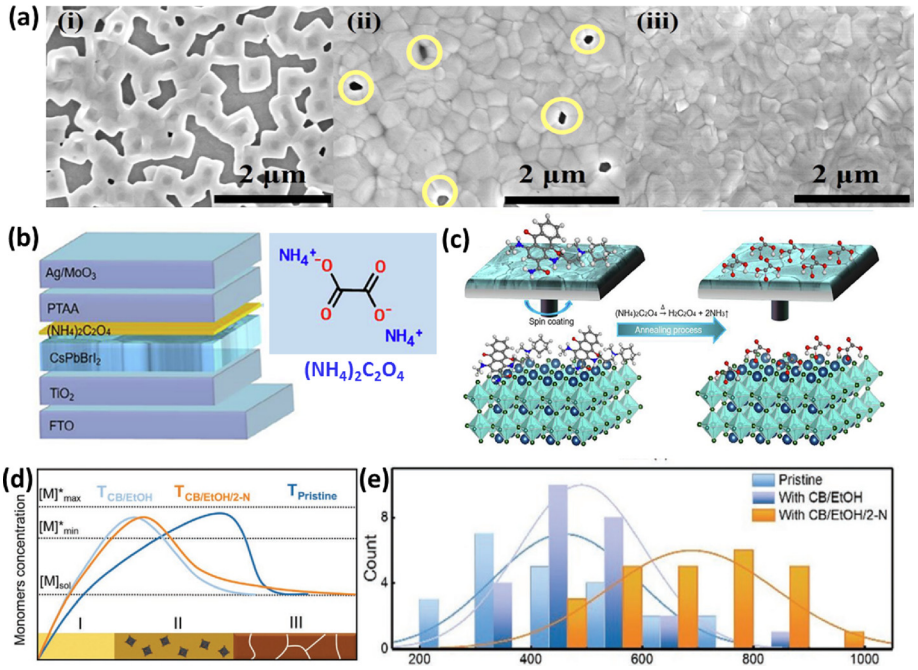

FIG. 3. ($a_{i–iii}$) Morphological images of $CsPbIBr_2$ films without anti-solvent treatment, with CB or diethyl ether treatment.[34] Reproduced with permission from Ghosh *et al.*, Appl. Surf. Sci. **592**, 152865 (2022). Copyright 2022 Elsevier. (b) Device structure of $CsPbBrI_2$-based IPVs, molecular structure of $(NH_4)_2C_2O_4$, and (c) schematic diagram of additive strategy.[35] Reproduced with permission from Wang *et al.*, Sci. Bull. **66**(4), 347–353 (2021). Copyright 2021 Elsevier. (d) LaMer diagram of nucleation and growth dynamics for AIP films without and with anti-solvent and/or 2-N, and (e) corresponding grain size distribution.[37] Reproduced with permission from Wang *et al.*, Adv. Energy Mater. **12**(31), 2201274 (2022). Copyright 2022 John Wiley and Sons.

Finkelstein reaction of inorganic perovskite film and generate a new phase. In the meanwhile, it coordinated with surface Pb^{2+} to form more stable Pb-Cl bonds. The synergistic effect suppresses defects of perovskite film surface. In addition, BCMS optimized energy level alignment to enhance charge extraction ability. The champion device achieved a PCE of 44.44% (V_{OC} = 1.056 V, J_{SC} =138 μA cm^2, FF = 84.9%) under 1000 lux WLED illumination.[49]

Recently reported IPV-performances based on interfacial strategies are summarized in Table III. These results underscore the critical importance of interface engineering in optimizing charge transport efficiency for IPV applications.

V. OTHERS

In addition to the above strategies, a variety of strategies have been applied to each component of AIP-based IPVs. Spiro-OMeTAD as a conventional hole-transporting material (HTM) for AIP-based devices usually requires an ionic dopant such as Li-TFSI to improve the hole mobility and conductivity, which, however, lowers the device stability due to unwanted ion migration.[50] To address this issue, T. Miyasaka designed a new polymer PDTDT with planar backbone [Figs. 5(a) and 5(c)] and applied it as dopant-free HTM. The PDTDT-based devices achieved indoor efficiencies up to 34.20% with a remarkable V_{OC} of 1.14 V.[51] In another work, Tan *et al.* studied a series of dopant-free conjugated polymers (P3HT, PBDB-T, and PM6) with different HOMO energy levels.[30] It was found that PM6 works better than the others due to its higher hole mobility as well as better matching between its HOMO and VBM levels of $CsPbI_2Br$. In addition, Zhu *et al.* performed multiple simulations on a series of inorganic HTMs (Cu_2O, CuI, CuSCN, $SrCu_2O_2$, $CuSbS_2$, $CuAlO_2$) [see Figs. 5(d) and 5(e)], showing that the devices with Cu_2O-HTL exhibit the best indoor performance due to minimized energy difference at the $CsPbI_2Br$/HTL/Au interfaces.[52] The optimal devices reached high efficiencies up to 34.02% under indoor conditions. Another critical strategy lies in tailoring the thickness of the absorber layer to enhance carrier transport efficiency. As evidenced by Wang *et al.*, $CsPb(I_{1-x}Br_x)_3$ films with precisely controlled thickness (i.e., 441 nm) exhibited relatively

TABLE II. Recently reported IPV-performances based on anti-solvent strategies.

Date	Device structure	V_{oc} (V)	J_{sc} (μA cm^{-2})	FF (%)	PCE (%)	Light source	Strategy	Ref.
2021	FTO/TiO_2/$CsPbBrI_2$/PTAA/MoO_3/Ag	0.75	170	62	28.48	FL 1000 lux	$(NH_4)_2C_2O_4H_2O$ in EtOH	35
2022	ITO/SnO_2/$CsPbIBr_2$/Spiro-OMeTAD/Au	0.95	60	61.6	14.1	WLED/6500 K 1000 lux	Diethyl ether as anti-solvent	34
2022	FTO/TiO_2/$CsPbI_3$/Spiro-OMeTAD/MoO_3/Ag	1.06	154	82	40.07	WLED/2956 K 1062 lux	Phthalimide (2-N) in CB/EtOH	37
2023	ITO/SnO_2/ZnO/$CsPbI_2Br$/P3HT/Au	1.051	110	76.79	23.24	WLED/3000 K 1000 lux	CFBA in IPA	36

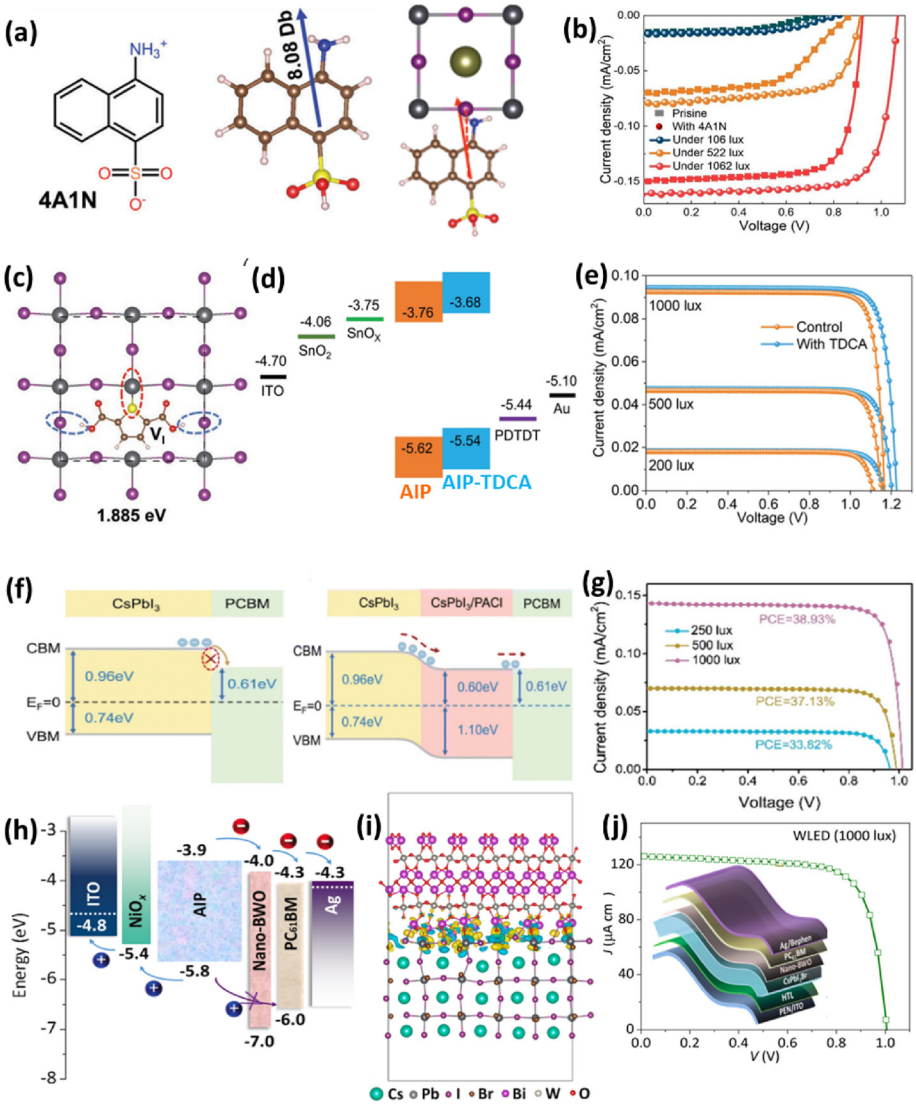

FIG. 4. (a) Molecular structure of 4A1N, its interaction with AIP, and (b) indoor *J–V* curves of the devices with 4A1N.[43] Reproduced with permission from Wang *et al.*, Adv. Mater. **35**(31), 2210106 (2023). Copyright 2023 John Wiley and Sons. (c) Interaction between TDCA and AIP defect (V_I), (d) energy diagram of IPV, and (e) indoor *J–V* curves of the devices.[45] Reproduced with permission from Guo *et al.*, Adv. Funct. Mater. **32**(43), 2207554 (2022). Copyright 2022 John Wiley and Sons. (f) Energy diagram of devices with PACl, and (g) indoor *J–V* curves.[46] Reproduced with permission from Wang *et al.*, Energy Environ. Sci. **16**(6), 2572–2578 (2023). Copyright 2023 Royal Society of Chemistry. (h) Energy diagram of inverted device with Nano-BWO, and (i) charge density difference at the α-$CsPbI_2Br$/Nano-BWO interface, and (j) indoor *J–V* curves of flexible device.[47] Reproduced with permission from Shu *et al.*, Chem. Eng. J. **466**, 143273 (2023). Copyright 2023 Elsevier.

better crystallinity compared with thinner and thicker films,[53] resulting in remarkable PCEs of 32.69% and 33.11% under FL and WLED illumination (1000 lux), respectively, highlighting the crucial role of thickness engineering in low-light energy harvesting.

On the other hand, compositional innovation through lead-free perovskites has emerged as a promising approach for IPVs. Notably, BiOI and $Cs_3Sb_2Cl_xI_{9-x}$ with wide bandgaps (1.90–1.95 eV) demonstrated exceptional environmental stability and spectral compatibility with indoor lighting.[54] The optimal devices incorporating these compositions achieved PCEs of 4.4% and 4.9%, respectively, under FL lighting (1000 lux), representing 4- to 5-fold enhancements compared to those (0.9% and 1.2%) under one-sun illumination. This performance inversion underscores the material-specific optimization requirements for indoor vs outdoor photovoltaic applications. A parallel study demonstrated the advantages of $Cs_2AgBiBr_6$ system, including superior crystallinity, extended carrier lifetimes (> 40 ns), and exceptional environmental resilience compared to lead-halide counterparts.[55] Theoretical simulations revealed that optimized devices with hydrogenated $Cs_2AgBiBr_6$ absorbers (with $E_g = 1.64$ eV) can attain a PCE of 24% under 2900 K illumination (200 lux). Further refinement through conduction band offset (CBO) optimization synergized with thickness and defect density control pushed the efficiency up to 41.03%, demonstrating the multi-parameter optimization potential in double perovskite systems. The above IPV-performances based on HTL and absorber strategies are listed in Table IV. These collective findings establish that both HTL design and absorber tuning constitute essential axes for advancing AIP-based IPVs.

VI. CONCLUSIONS AND PROSPECTIVE

In summary, AIPs are found to be ideal candidates for IPV applications, owing to their tunable bandgap alignment with indoor spectra, superior stability across diverse operational conditions, and

TABLE III. Recently reported IPV-performances based on interfacial strategies.

Date	Device structure	V_{oc} (V)	J_{sc} (μA cm^{-2})	*FF* (%)	PCE (%)	Light source	Strategy	Ref.
2021	ITO/SnO_2/$CsPbI_2Br$/P3CT/TFB/P3HT/Au	0.94	133.74	68	27.47	WLED/6500 K 1000 lux	P3CT treatment	41
2022	ITO/SnO_2/SnO_x/$CsPbI_{2.25}Br_{0.75}$ (TDCA)/PDTDT/Ag	1.17/1.20/1.23	18.44/47.37/95.54	83/84/84	29.56/31.72/32.41	WLED/5000 K 200/500/1000 lux	TDCA treatment	45
2023	FTO/NiO_x/$CsPbI_2Br$/PAMAM/ZnO@C_{60}/Ag	1.06	109.6	84.39	35.71	FL 1000 lux	PAMAM treatment	42
2023	FTO/TiO_2/4A1N/$CsPbI_3$/Spiro-OMeTAD/MoO_3/Ag	0.83/0.91/1.07	16/77/155	74/78/83	29.45/32.54/**41.21**	WLED/2956 K 106/522/1062 lux	4A1N treatment	43
2023	FTO/TiO_2/$CsPbI_{3-x}Br_x$/Spiro-OMeTAD/Au	1.012	172.58	77.66	39.78	Cool WLED 1200 lux	TFA treatment	44
2023	FTO/P3CT/$CsPbI_3$/PACl/$PC_{61}BM$/BCP/Ag	0.97/0.99/1.02	32.9/70.1/143	81/82/82	33.82/37.13/38.93	Warm WLED 250/500/1000 lux	PACl treatment	46
2023	ITO/NiO_x/$CsPbI_2Br$/Nano-BWO/$PC_{61}BM$/Bphen/Ag	1.041	137	80.62	30.43	WLED/6500 K 1000 lux	Nano-BWO treatment	47
2025	FTO/NiO_x/MeO-2PACz/$CsPbI_{3-x}Br_x$/[6,6]-PCBM/BCP/Ag	1.056	138	84.9	44.44	WLED 1000 lux	BCMS treatment	49

compatibility with rigid and flexible substrates. To date, the state-of-the-art IPVs based on AIPs have achieved champion PCEs exceeding 40% under indoor illumination. Nevertheless, several critical challenges still remain to be addressed to facilitate practical implementation:

(i) AIP-based IPVs more often exhibit significant energy losses, primarily manifested as low open-circuit voltages ($V_{OC} < 1.0$ V) and diminished voltage outputs. This limitation stems from non-uniform nucleation and rapid crystallization during AIP film formation, which yields defective perovskite layers characterized by pin-holes and small grains. These structural imperfections induce severe carrier recombination, particularly detrimental under photon-starved indoor conditions where recombination losses disproportionately degrade performance. To address AIP film quality, organic additives with passivation groups have been employed; however, residual additives often impede carrier mobility. While co-solvents (e.g., DMSO) and volatile additives (e.g., DMAI) can regulate crystallization and evaporate during annealing, their complete removal necessitates high annealing temperatures, which precludes their use in temperature-sensitive flexible wearable electronics. To circumvent the annealing constraints, introducing anti-solvents with a low boiling point would be an effective strategy, which enables additive extraction and crystallization regulation at reduced temperature. Thus, combining additive and anti-solvent strategies generates synergistic benefits: simultaneous crystallization control and defect passivation could be achieved without compromising carrier mobility. Nevertheless, anti-solvent toxicity and compatibility with scalable manufacturing processes still remain challenging.

(ii) Another source of energy loss in AIP-based IPVs stems from interfacial properties, including high defect density at the AIP film surface and energy level mismatch between AIP and adjacent carrier transport layers. The top surface defects of AIP films can be passivated by facile post-treatment. In comparison, due to the thermal expansion coefficient and lattice mismatch between the AIP layer and the buried layer, the bottom surface of AIP is even more defective. Nevertheless, the inaccessibility of this buried interface precludes conventional post-treatment strategies, severely limiting defect passivation opportunities. Moreover, the energy level mismatch between AIP and charge transport layers constitutes another critical bottleneck, causing severe voltage losses and device instability. To address these issues, strategic modifications or gradient heterojunctions shall be engineered at the buried interface to mitigate interfacial defects and optimize interfacial band alignment.

(iii) The indoor performance of flexible devices needs to be improved to realize lightweight, conformal photovoltaic systems for wearable electronics. Furthermore, inverted (p-i-n) configurations demonstrate inherent stability advantages through dopant-free charge transport layers and compatibility with silicon-based devices to fabricate tandem solar cells to break through the S-Q efficiency limit. However, their IPV performance (e.g., typical device based on NiO_x) lags behind those with normal structures due to interface defect-induced non-radiative recombination, low charge extraction

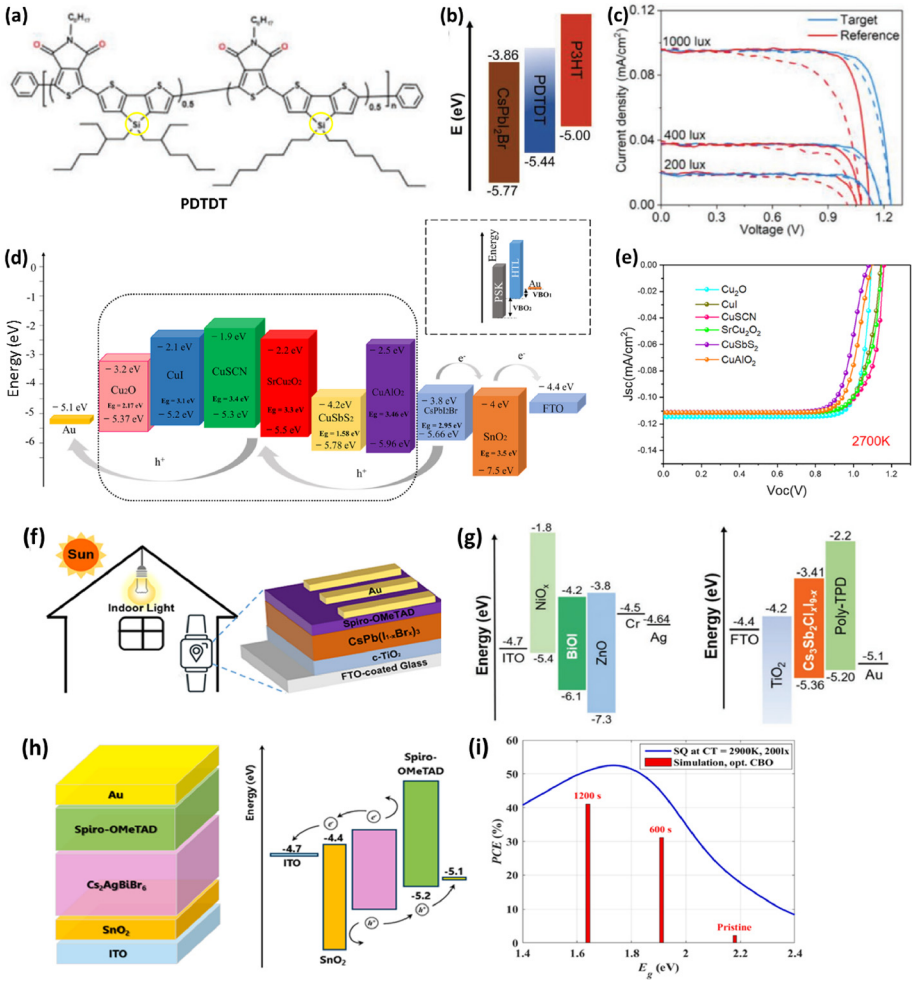

FIG. 5. (a) Molecular structure of PDTDT, (b) energy diagram of $CsPbI_2Br$/HTL, and (c) *J–V* curves of IPV with dopant-free HTL.[51] Reproduced with permission from Guo *et al.*, Adv. Funct. Mater. **31**(42), 2103614 (2021). Copyright 2021 John Wiley and Sons. (d) Energy diagram of $CsPbI_2Br$/HTLs, and (e) simulated *J–V* curves of optimal IPVs with different HTLs.[52] Reproduced with permission from Liu *et al.*, Opt. Quantum Electron. **56**(3), 281 (2024). Copyright 2024 Springer Nature. (f) Schematic structure of IPV based on $CsPb(I_{1-x}Br_x)_3$.[53] Reproduced with permission from Wang *et al.*, ACS Appl. Mater. Interfaces **14**(9), 11528–11537 (2022). Copyright 2022 American Chemical Society. (g) Energy diagram of IPVs based on BiOI or $Cs_3Sb_2Cl_xI_{9-x}$.[54] (h) Schematic structure of IPV based on $Cs_2AgBiBr_6$ and energy diagram. (i) Comparison between theoretical S-Q efficiency limit and simulation results.[55] Reproduced with permission from Alanazi *et al.*, J. Alloy. Compd. **1010**, 177354 (2025). Copyright 2025 Elsevier.

TABLE IV. Recently reported IPV-performances based on HTL and absorber strategies.

Date	Device structure	V_{oc} (V)	J_{sc} (μA cm^{-2})	FF (%)	PCE (%)	Light source	Strategy	Ref.
2020	ITO/NiO_x/BiOI/ZnO/Cr/Ag and ITO/NiO_x/$Cs_3Sb_2Cl_xI_{9-x}$/ZnO/Cr/Ag	0.60/0.60 and 0.49/0.47	56/62 and 82/76	38/40 and 42/40	4.0/4.4 and 4.9/4.4	FL/WLED/6500 K 1000 lux	Lead-free absorber	54
2021	ITO/SnO_2/SnO_X/$CsPbI_2Br$/PDTDT/Au	1.14	20.96	86	34.20	WLED 200 lux	Dopant-free PDTDT	51
2022	FTO/TiO_2/$CsPb(I_{1-x}Br_x)_3$/Spiro-OMeTAD/Au	0.985/0.999	128.19/117.96	80.26/80.36	32.69/33.11	FL/WLED/6500 K 1000 lux	Regulate thickness of $CsPbI_3$ layer	53
2022	ITO/SnO_2/$CsPbI_2Br$:$Pb(Ac)_2$/PM6/MoO_3/Ag	1.15	118	82	33.68	WLED/3000 K 1000 lux	P3HT, PBDB-T and PM6	30
2023	ITO/SnO_2/$CsPbI_2Br$/HTL/Au	1.107	118	83	34.02	WLED/2700 K 1000 lux	Cu_2O,CuI,CuSCN, $SrCu_2O_2$,$CuSbS_2$, $CuAlO_2$	52
2025	ITO/SnO_2/$Cs_2AgBiBr_6$/Spiro-OMeTAD/Au	⋯	⋯	⋯	41.03 (sim.)	WLED/2900 K 200 lux	Lead-free absorber	55

efficiency, and energy level mismatch. In addition, though lead-free alternatives currently exhibit inferior indoor efficiency (< 5%), their development remains crucial for sustainable technology deployment. Alternatively, hybrid strategies incorporating lead-reduced compositions and encapsulation technologies may balance efficiency with environmental safety.

Addressing these challenges requires synergistic efforts in materials engineering, device physics understanding, and system-level optimization. Emerging opportunities lie in machine learning-assisted bandgap engineering, self-powered IoT system integration, and scalable manufacturing processes. With continuous multidisciplinary innovation, AIP-based IPVs are poised to become cornerstone technologies in the evolving landscape of power supply for IoTs in the near future.

ACKNOWLEDGMENTS

The authors acknowledge receiving financial support from the National Science Foundation of Jiangsu province of China (BK20231312), the National Natural Science Foundation of China (52172050 and 52073197), and the Science Research Project of Jiangsu Higher Education Institutions (21KJA480002).

AUTHOR DECLARATIONS

Conflict of Interest

The authors have no conflicts to disclose.

Author Contributions

Yu Qi: Data curation (lead); Investigation (lead); Resources (lead); Supervision (equal); Validation (lead); Visualization (lead); Writing – review & editing (equal). **Wenjie Xu:** Conceptualization (equal); Data curation (equal); Investigation (equal); Resources (equal). **Yanhui Lou:** Conceptualization (equal); Formal analysis (equal); Methodology (equal); Project administration (equal); Supervision (equal); Validation (equal). **Lai Feng:** Conceptualization (lead); Data curation (equal); Formal analysis (equal); Methodology (lead); Project administration (equal); Writing – original draft (lead); Writing – review & editing (equal).

DATA AVAILABILITY

The data that support the findings of this study are available within this article.

REFERENCES

[1]K. S. Srivishnu, P. R. Markapudi, S. Sundaram, and L. Giribabu, "Semitransparent perovskite solar cells for building integrated photovoltaics: Recent advances," Energies **16**(2), 889 (2023).
[2]K. S. Srivishnu, M. N. Rajesh, S. Prasanthkumar, and L. Giribabu, "Photovoltaics for indoor applications: Progress, challenges and perspectives," Sol. Energy **264**, 112057 (2023).
[3]F. C. Chen, "Emerging organic and organic/inorganic hybrid photovoltaic devices for specialty applications: Low-level-lighting energy conversion and biomedical treatment," Adv. Opt. Mater. **7**(1), 1800662 (2019).
[4]A. A. Goje, N. A. Ludin, P. N. A. Fahsyar, U. Syafiq, P. Chelvanathan, A. D. A. Syakirin, M. A. Teridi, M. A. Ibrahim, M. S. Su'ait, S. Sepeai, and A. S. H. M. Yasir, "Review of flexible perovskite solar cells for indoor and outdoor applications," Mater. Renewable Sustainable Energy **13**(1), 155–179 (2024).
[5]K. Wang, Y. Zhou, Y. Lou, and Z. Wang, "Perovskite indoor photovoltaics: Opportunity and challenges," Chem. Sci. **12**(36), 11936–11954 (2021).
[6]X. Zhu, J. Xu, H. Cen, Z. Wu, H. Dong, and J. Xi, "Perspectives for the conversion of perovskite indoor photovoltaics into IoT reality," Nanoscale **15**(11), 5167–5180 (2023).
[7]B. Yan, X. Liu, W. Lu, M. Feng, H. Yan, Z. Li, S. Liu, C. Wang, J. Hu, and D. Xue, "Indoor photovoltaics awaken the world's first solar cells," Sci. Adv. **8**(49), eadc9923 (2022).
[8]P. Kumari, S. Prasanthkumar, and L. Giribabu, "Recent progress on perovskite based indoor photovoltaics: Challenges and commercialization," Sol. Energy **284**, 113049 (2024).
[9]B. Li, M. Lu, J. Feng, J. Zhang, P. M. Smowton, J. I. Sohn, I. Park, H. Zhong, and B. Hou, "Colloidal quantum dot hybrids: An emerging class of materials for ambient lighting," J. Mater. Chem. C **8**(31), 10676–10695 (2020).
[10]B. Li, B. Hou, and G. A. J. Amaratunga, "Indoor photovoltaics, the next big trend in solution-processed solar cells," InfoMat **3**(5), 445–459 (2021).
[11]T. Saga, "Advances in crystalline silicon solar cell technology for industrial mass production," NPG Asia Mater. **2**(3), 96–102 (2010).
[12]W. Chi and S. K. Banerjee, "Comparison and integration of CuInGaSe and perovskite solar cells," J. Energy Chem. **78**, 463–475 (2023).
[13]Q. Wu, C. Xue, Y. Li, P. Zhou, W. Liu, J. Zhu, S. Dai, C. Zhu, and S. Yang, "Kesterite Cu_2ZnSnS_4 as a low-cost inorganic hole-transporting material for high-efficiency perovskite solar cells," ACS Appl. Mater. Interfaces **7**(51), 28466–28473 (2015).
[14]J. K. W. Ho, H. Yin, and S. K. So, "From 33% to 57% an elevated potential of efficiency limit for indoor photovoltaics," J. Mater. Chem. A **8**(4), 1717–1723 (2020).
[15]C. Polyzoidis, K. Rogdakis, and E. Kymakis, "Indoor perovskite photovoltaics for the internet of things—Challenges and oppportunities toward market uptake," Adv. Energy Mater. **11**(38), 2101854 (2021).
[16]A. J. Knight, A. D. Wright, J. B. Patel, D. P. Mcmeekin, H. J. Snaith, M. B. Johnston, and L. M. Herz, "Electronic traps and phase segregation in lead mixed-halide perovskite," ACS Energy Lett. **4**(1), 75–84 (2019).
[17]X. Y. Li, Q. Sun, Y. M. Xie, and M. K. Fung, "All-inorganic perovskite solar cells: Modification strategies and challenges," Adv. Energy Sustainability Res. **5**(6), 2300263 (2024).
[18]Z. Wang, Q. Chen, H. Xie, X. Feng, Y. Du, T. Zhou, R. Li, J. Zhang, L. Zhang, Z. Xu, L. Xi, Q. Tian, and S. F. Liu, "Light-driven dynamic defect-passivation for efficient inorganic perovskite solar cells," Adv. Funct. Mater. **35**(9), 2416118 (2025).
[19]X. Wang, A. M. Ganose, S. R. Kavanagh, and A. Walsh, "Band versus polaron: Charge transport in antimony chalcogenides," ACS Energy Lett. **7**, 2954–2960 (2022).
[20]G. K. Grandhi, G. Koutsourakis, J. C. Blakesley, F. D. Rossi, F. Brunetti, S. Öz, A. Sinicropi, M. L. Parisi, T. M. Brown, M. J. Carnie, R. L. Z. Hoye, and P. Vivo, "Promises and challenges of indoor photovoltaics," Nat. Rev. Clean Technol. **1**, 132–147 (2025).
[21]X. Liu, S. Xu, B. Tang, and X. Song, "Indoor organic photovoltaics for low-power internet of things devices: Recent advances, challenges, and prospects," Chem. Eng. J. **497**, 154944 (2024).
[22]K. S. Kim, I. S. Jin, S. H. Park, S. J. Lim, and J. W. Jung, "Methylammonium iodide-mediated controlled crystal growth of $CsPbI_2Br$ films for efficient and stable all-inorganic perovskite solar cells," ACS Appl. Mater. Interfaces **12**(32), 36228–36236 (2020).
[23]I. S. Jin, B. Parida, and J. W. Jung, "Simultaneously enhanced efficiency and ambient stability of inorganic perovskite solar cells by employing tetramethylammonium chloride additive in $CsPbI_2Br$," J. Mater. Sci. Technol. **102**, 224–231 (2022).
[24]J. Bahadur, S. W. Cho, P. Pandey, S. Yoon, D. G. Lee, J. Ryu, J. T. Song, J. Lim, and D. W. Kang, "Mitigating defect states of all-Inorganic $CsPbI_2Br$ perovskite via multifunctional 2-Amino-5-Nitrothiazole additive for an efficient air-processed outdoor/indoor photovoltaics," Sol. RRL **8**(5), 2300912 (2024).
[25]S. Choi, H. J. Lee, J. H. Heo, and S. H. Im, "Efficient inorganic $CsPbI_2Br$ perovskite indoor photovoltaics demonstrated via slower crystallization by incorporated dimethylammonium iodide," EcoMat **5**(3), e12303 (2023).
[26]Y. Du, Q. Tian, X. Chang, J. Fang, X. Gu, X. He, X. Ren, K. Zhao, and S. F. Liu, "Ionic liquid treatment for highest-efficiency ambient printed stable all-inorganic $CsPbI_3$ perovskite solar cells," Adv. Mater. **34**(10), 2106750 (2022).

[27]M. H. Li, X. Gong, S. Wang, L. Li, J. Fu, J. Wu, Z. Tan, and J. S. Hu, "Facile hydrogen-bonding assisted crystallization modulation for large-area high-quality $CsPbI_2Br$ films and efficient solar cells," Angew. Chem. **136**(10), e202318591 (2024).
[28]W. Xu, J. Xiong, Q. Yuan, W. Xu, Q. Shu, Y. Lou, and L. Feng, "Cytidylic acid improves crystal growth, defect passivation and flexibility of inorganic $CsPbI_2Br$ film for inverted photovoltaics towards versatile applications," Chem. Eng. J. **480**, 147946 (2024).
[29]I. S. Jin, K. S. Kim, and J. W. Jung, "CsCl-induced defect control of $CsPbI_2Br$ thin films for achieving open-circuit voltage of 1.33 V in all-inorganic perovskite solar cells," J. Power Sources **512**, 230481 (2021).
[30]S. Jiang, Y. Bai, Z. Xu, F. Wang, L. Xia, Y. Yang, C. Li, and Z. Tan, "Efficient perovskite indoor photovoltaics with open-circuit voltage of 1.15 V via collaborative optimization of $CsPbI_2Br$ layer and hole transport layer," Small Methods **6**(10), 2200624 (2022).
[31]C. Dong, X. Han, W. Li, Q. Qiu, and J. Wang, "Anti-solvent assisted multi-step deposition for efficient and stable carbon-based CsPbI2Br all-inorganic perovskite solar cell," Nano Energy **59**, 553–559 (2019).
[32]J. Yang, H. Yu, S. Wu, C. Cai, J. Gao, X. Lu, X. Gao, L. Shui, S. Wu, and J. Liu, "A mixed antisolvent-assisted crystallization strategy for efficient all-inorganic $CsPbIBr_2$ perovskite solar cells by a low-temperature process," ACS Appl. Energy Mater. **5**(3), 2881–2889 (2022).
[33]T. Moot, A. R. Marshall, L. M. Wheeler, S. N. Habisreutinger, T. H. Schloemer, C. C. Boyd, D. R. Dikova, G. F. Pach, A. Hazarika, M. D. Mcgehee, H. J. Snaith, and J. M. Luther, "CsI-antisolvent adduct formation in all-inorganic metal halide perovskites," Adv. Energy Mater. **10**(9), 1903365 (2020).
[34]P. Ghosh, J. Bruckbauer, C. Trager-Cowan, and L. Krishnan Jagadamma, "Crystalline grain engineered $CsPbIBr_2$ films for indoor photovoltaics," Appl. Surf. Sci. **592**, 152865 (2022).
[35]K. Wang, X. Li, Y. Lou, M. Li, and Z. Wang, "$CsPbBrI_2$ perovskites with low energy loss for high-performance indoor and outdoor photovoltaics," Sci. Bull. **66**(4), 347–353 (2021).
[36]J. Bahadur, S. Cho, P. Pandey, J. Ryu, S. Yoon, D. Lee, J. T. Song, J. S. Cho, and D. Kang, "Surface defect passivation of all-inorganic $CsPbI_2Br$ perovskites via fluorinated ionic liquid for efficient outdoor/indoor photovoltaics processed in ambient air," Appl. Surf. Sci. **637**, 157901 (2023).
[37]K. L. Wang, Z. H. Su, Y. H. Lou, Q. Lv, J. Chen, Y. R. Shi, C. H. Chen, Y. H. Zhou, X. Y. Gao, Z. K. Wang, and L. S. Liao, "Rapid nucleation and slow crystal growth of $CsPbI_3$ films aided by solvent molecular sieve for perovskite photovoltaics," Adv. Energy Mater. **12**(31), 2201274 (2022).
[38]J. He, J. Su, J. Di, Z. Lin, S. Zhang, J. Ma, J. Zhang, S. Liu, J. Chang, and Y. Hao, "Surface reconstruction strategy improves the all-inorganic $CsPbIBr_2$ based perovskite solar cells and photodetectors performance," Nano Energy **94**, 106960 (2022).
[39]J. Sun, Y. Jin, Q. Liu, and F. Qiu, "Surface-modification-induced synergies of crystal growth and defect passivation toward CsPbI2Br solar cells with efficiency exceeding 17%," Chem. Eng. J. **457**, 141300 (2023).
[40]J. He, Q. Wang, Y. Xu, X. Guo, L. Zhou, J. Su, Z. Lin, J. Zhang, Y. Hao, and J. Chang, "Synergistic effect of surface p-doping and passivation improves the efficiency, stability, and reduces lead leakage in all-inorganic $CsPbIBr_2$ -based perovskite solar cells," Small **19**(6), e2205962 (2023).
[41]Y. Chung, K. S. Kim, and J. W. Jung, "On the role of carboxylated polythiophene in defect passivation of $CsPbI_2Br$ surface for efficient and stableall-inorganic perovskite solar cells," Int. J. Energy Res. **46**(5), 6012–6021 (2022).
[42]M. Ma, Y. Zeng, Y. Yang, C. Zhang, Y. Ma, S. Wu, C. Liu, and Y. Mai, "Dendrimer modification strategy based on the understanding of the photovoltaic mechanism of a perovskite device under full sun and indoor light," ACS Appl. Mater. Interfaces **15**(21), 25550–25557 (2023).
[43]K. L. Wang, H. Lu, M. Li, C. H. Chen, D. Bo Zhang, J. Chen, J. J. Wu, Y. H. Zhou, X. Q. Wang, Z. H. Su, Y. R. Shi, Q. S. Tian, Y. X. Ni, X. Y. Gao, S. M. Zakeeruddin, M. Grätzel, Z. K. Wang, and L. S. Liao, "Ion–dipole interaction enabling highly efficient $CsPbI_3$ perovskite indoor photovoltaics," Adv. Mater. **35**(31), 2210106 (2023).
[44]H. Zhang, W. Xiang, X. Zuo, X. Gu, S. Zhang, Y. Du, Z. Wang, Y. Liu, H. Wu, P. Wang, Q. Cui, H. Su, Q. Tian, and S. F. Liu, "Fluorine-containing passivation layer via surface chelation for inorganic perovskite solar cells," Angew. Chem., Int. Ed. **62**(6), e202216634 (2023).
[45]Z. Guo, S. Zhao, N. Shibayama, A. Kumar Jena, I. Takei, and T. Miyasaka, "A universal method of perovskite surface passivation for $CsPbX_3$ solar cells withV_{OC} over 90% of the S-Q limit," Adv. Funct. Mater. **32**(43), 2207554 (2022).
[46]S. Wang, M. Li, Y. Zhang, Y. Jiang, L. Xu, F. Wang, and J. Hu, "Surface n-type band bending for stable inverted $CsPbI_3$ perovskite solar cells with over 20% efficiency," Energy Environ. Sci. **16**(6), 2572–2578 (2023).
[47]Q. Shu, J. Xiong, B. Zhu, W. Xu, W. Xu, K. You, G. Chen, Y. Lou, and L. Feng, "Constructing graded heterojunctions for rigid and flexible inverted photovoltaics under outdoor and indoor illumination," Chem. Eng. J. **466**, 143273 (2023).
[48]D. Han, S. Yi, Q. Yuan, X. Tang, Q. Shu, Q. Li, F. Wang, D.-Y. Zhou, and L. Feng, "Managing defects density and interfacial strain via underlayer engineering for inverted $CsPbI_2Br$ perovskite solar cells with all-layer dopant-free," Small **17**(28), 2101902 (2021).
[49]T. Xu, S. Liu, S. Seok II, and W. Xiang, "Surface chemistry-induced reconstruction of inorganic perovskites for efficient and stable inverted solar cells," Joule **9**(4), 101826 (2025).
[50]Z. Fan, Y. Duan, M. Wu, H. Zou, Y. Yao, Y. Li, D. Xu, J. Tan, Y. Li, H. Wang, Y. Wang, Z. Xie, H. Lei, Z. Wang, T. Zhao, Q. Peng, S. Liu, and Z. Liu, "High open-circuit voltage and efficiency $CsPbI_3$ perovskite solar cells achieved by hole transport layer modification," Adv. Energy Mater. **15**, 2405360 (2024).
[51]Z. Guo, A. K. Jena, I. Takei, M. Ikegami, A. Ishii, Y. Numata, N. Shibayama, and T. Miyasaka, "Dopant-free polymer HTM-based $CsPbI_2Br$ solar cells with efficiency over 17% in sunlight and 34% in indoor light," Adv. Funct. Mater. **31**(42), 2103614 (2021).
[52]G. Liu, C. Lin, X. Xi, L. Wang, Q. Wang, S. Jin, H. Zhou, D. Xu, B. Zhu, and J. Zhu, "Numerical analysis of all-inorganic perovskite solar cells with different Cu-based hole transport layers under indoor illuminations," Opt. Quantum Electron. **56**(3), 281 (2024).
[53]M. Wang, Q. Wang, J. Zhao, Y. Xu, H. Wang, X. Zhou, S. Yang, Z. Ci, and Z. Jin, "Low-trap-density $CsPbX_3$ film for high-efficiency indoor photovoltaics," ACS Appl. Mater. Interfaces **14**(9), 11528–11537 (2022).
[54]Y. Peng, T. N. Huq, J. Mei, L. Portilla, R. A. Jagt, L. G. Occhipinti, J. L. Macmanus Driscoll, R. L. Z. Hoye, and V. Pecunia, "Lead-free perovskite-inspired absorbers for indoor photovoltaics," Adv. Energy Mater. **11**(1), 2002761 (2021).
[55]T. I. Alanazi, A. Shaker, and D. Selim, "Performance analysis of hydrogenated $Cs_2AgBiBr_6$ perovskite solar cells under white LED illumination," J. Alloy. Compd. **1010**, 177354 (2025).